

Lower bounds on entanglement entropy without twin copy

Yannick Meurice

Department of Physics and Astronomy, The University of Iowa, Iowa City, IA 52242, USA

(Dated: April 4, 2025)

We discuss the possibility of estimating experimentally the von Neumann entanglement entropy S_A^{vN} of a symmetric bi-partite quantum system AB by using the basic measurement counts (bitstrings) for a *single* copy of a prepared state. Using exact diagonalization and analog simulations performed with the publicly available QuEra facilities for chains and ladders of Rydberg atoms, we calculate the Shannon entropy S_{AB}^X associated with the bitstrings of adiabatically prepared ground states and the reduced entropies S_A^X and S_B^X obtained from the marginal probabilities in A and B . We then calculate the classical mutual information $I_{AB}^X = S_A^X + S_B^X - S_{AB}^X$, which is a lower bound on S_A^{vN} . We show that for a broad range of lattice spacing and detuning, I_{AB}^X is typically 20 percent below S_A^{vN} in regions where S_A^{vN} is large and a less close bound in regions where S_A^{vN} is low. We argue that this use of the easily available bitstrings provides a robust and efficient way to explore empirically the phase diagram of qubit-based quantum simulators and identify critical regions.

Introduction. Entanglement entropy is a crucial theoretical concept in quantum physics with applications for many-body physics [1–4], gauge theory [5–8], high-energy collisions [9–11], nuclear physics [12, 13] and studies of conformal field theory [14–17]. It provides important information regarding quantum phases transitions. However, the experimental measurement of entanglement entropy is notoriously difficult due to its nonlocal nature. This led to the idea of coupling several copies of the original system [18]. A standard proposal is to measure the second order Rényi entropy S_2 by performing a swap operation between twin copies of a system [19]. Cold atom experimentalists [20, 21] were able to prepare and interfere twin copies of a state in small optical lattices to measure S_2 . If practically feasible for larger systems, this would allow the experimental measurement of the central charge which is an important characterization of conformal systems [14–16, 22].

Preparing and interfering twin copies of a quantum system are not easy experimental tasks. On the other hand, a generic qubit-based quantum computing device provides counts for bitstrings often given as python dictionaries. For instance, for 1000 shots with a two-qubit universal quantum computer one gets counts for the four possible states in the form {'01': 269, '00': 251, '10': 247, '11': 233}. As another example, for a 10 Rydberg atom analog simulator where g and r represent, for each atom, the ground and Rydberg states respectively the counts are given as {'gggrgrgrgr': 8, 'rgrrgrgrgr': 160, ...}. By dividing these counts by the total number of shots, we can estimate the probabilities $p_{\{n\}}$ for the bitstring states $|\{n\}\rangle$. We can then introduce an AB bipartition and calculate the marginal probabilities in A or B . For instance in the 10 atom example, we can estimate the probability to observe **grgrgr** on the right side of a chain irrespectively of the observations made in B . This reduction process is reminiscent of the tracing over a subsystem used to calculate the von Neumann quantum entanglement S_A^{vN} which is equal to S_B^{vN} for a pure state.

In this Letter, we discuss the applications of concepts introduced by Shannon [23] in the context of the transmission and interpretation of classical bits, to the bitstring measurements of bipartite quantum systems. Using the Shannon entropy associated with these bitstrings and reduced versions obtained from the marginal probabilities, it is easy to calculate the classical mutual information I_{AB}^X , which is a lower bound on S_A^{vN} [24, 25]. We show that for a broad range of tunable parameters, I_{AB}^X is typically 20 percent below S_A^{vN} in regions where S_A^{vN} is large and a less close bound in regions where S_A^{vN} is low. In other words, I_{AB}^X provides unexpectedly good characterizations of the variations of S_A^{vN} and allows an efficient exploration of phase diagrams. The bitstrings are available on many analog and universal quantum computing platforms. In the following, we focus on configurable arrays of Rydberg atoms. We used exact diagonalization and conducted analog simulations using the QuEra device Aquila [26] which is publicly available and can be operated with limited resources.

The presentation is organized as follows. We introduce the bitstring Shannon entropy and mutual information for a bipartite quantum system and then perform calculations for a chain of 10 Rydberg atoms with a fixed detuning to Rabi frequency ratio Δ/Ω and a variable lattice spacing. We then extend the numerical calculations for a broad range of Δ/Ω and more general situations.

Bi-partite setup, bitstring mutual information and quantum bounds. In the following we focus on the vacuum density matrix $\rho_{AB} = |vac.\rangle\langle vac. |$ of a bipartite AB quantum system. We define the reduced density matrix $\rho_A = \text{Tr}_B \rho_{AB}$ and the von Neumann entanglement entropy

$$S_A^{vN} \equiv -\text{Tr}(\rho_A \ln(\rho_A)), \quad (1)$$

which is independent of the bases used in A and B . We now express ρ_{AB} in the computational basis which has a bipartite factorization $|\{n\}_{AB}\rangle = |\{n\}_A\rangle |\{n\}_B\rangle$. In this basis, the diagonal elements are the probabilities for the bitstrings. The Shannon entropy for the experimental

probabilities is defined as:

$$S_{AB}^X \equiv - \sum_{\{n\}} p_{\{n\}} \ln(p_{\{n\}}). \quad (2)$$

The superscript X is short for eXperimental as opposed to quantum von Neuman (or Rényi).

Similarly, we can consider the diagonal part of ρ_A . Since the partial tracing over B is a diagonal operation, the reduced diagonal elements

$$p_{\{n\}_A} = \sum_{\{n\}_B} p_{\{n\}_A\{n\}_B}, \quad (3)$$

are the marginal probabilities introduced in the 18th century and we define the reduced experimental entropy

$$S_A^X \equiv - \sum_{\{n\}_A} p_{\{n\}_A} \ln(p_{\{n\}_A}). \quad (4)$$

This quantity is basis dependent and its relation to the basis independent S_A^{vN} can in general be expressed as an upper bound using convexity arguments [25, 27]:

$$S_A^{vN} \leq S_A^X \quad (5)$$

The process can be repeated for ρ_B leading to S_B^X . In general, $S_B^X \neq S_A^X$ as it can be easily seen by taking A and B with very different sizes. This is contrast to the quantum symmetry $S_B^{vN} = S_A^{vN}$ for a pure state.

Shannon [23] introduced a manifestly $A - B$ symmetric, non-negative, quantity usually called the mutual information I_{AB} which is a measure of the information shared by A and B . In our bitstring context, it reads:

$$I_{AB}^X = S_A^X + S_B^X - S_{AB}^X. \quad (6)$$

It is clear that in the limit where $p_{\{n\}} = p_{\{n\}_A} p_{\{n\}_B}$, the measurements in A and B are completely unrelated and $I_{AB}^X = 0$. At the quantum level, if the pure state is a product of two states in A and B , then $S_B^{vN} = S_A^{vN} = 0$. This suggests that there could exist a relation between I_{AB}^X and S_A^{vN} . We first empirically observed that I_{AB}^X was keeping track of S_A^{vN} from below and it was pointed out to us [28] that a general inequality can be obtained from the Holevo bound discussed in [24, 25]:

$$I_{AB}^X \leq S_A^{vN} = S_B^{vN} \quad (7)$$

In summary, we have provided upper and lower bounds on the von Neumann entanglement that can be easily obtained from bitstring data. The main question addressed hereafter is to decide if some of these bounds can be tight enough to provide reliable information about quantum entanglement.

In the rest of this Letter, we assume that A and B have the same size and can be interchanged by a reflection symmetry. This implies that $S_A^X = S_B^X$ and $I_{AB}^X = 2S_A^X - S_{AB}^X$. Applications in asymmetric cases work well and are discussed elsewhere [29, 30].

Rydberg atoms setup. Recently, optical tweezer have been used to create arrays of Rydberg atoms with adjustable geometries [31–36]. Their Hamiltonian reads

$$H = \frac{\Omega}{2} \sum_i (|g_i\rangle \langle r_i| + |r_i\rangle \langle g_i|) - \Delta \sum_i n_i + \sum_{i < j} V_{ij} n_i n_j, \quad (8)$$

with van der Waals interactions $V_{ij} = \Omega R_b^6 / r_{ij}^6$, for a distance r_{ij} between the atoms labelled as i and j . By definition, $r_{ij} = R_b$, the Rydberg blockade radius, when $V_{ij} = \Omega$ the Rabi frequency. We define the Rydberg occupation $n_i |r_i\rangle = |r_i\rangle$ while $n_i |g_i\rangle = 0$. In the following we use $\Omega = 5\pi$ MHz, which implies $R_b = 8.375\mu\text{m}$, and a detuning $\Delta = 17.5\pi$ MHz as in [37]. We will consider chains and ladders of atoms with varying lattice spacings. The adiabatic preparation is discussed in Appendix A and the errors on the bitstring measurements in Appendix B.

Numerical calculations. As a first step to understand the connections among the bitstring entropies and S_A^{vN} , we consider the ground state of a chain of 10 Rydberg atoms separated by a varied lattice spacing a_x expressed in units of R_b . A and B are the left and right sides with 5 atoms each. We used exact diagonalization to calculate S_{AB}^X , S_A^X , I_{AB}^X , and S_A^{vN} for the vacuum. The results are shown in Fig. 6.

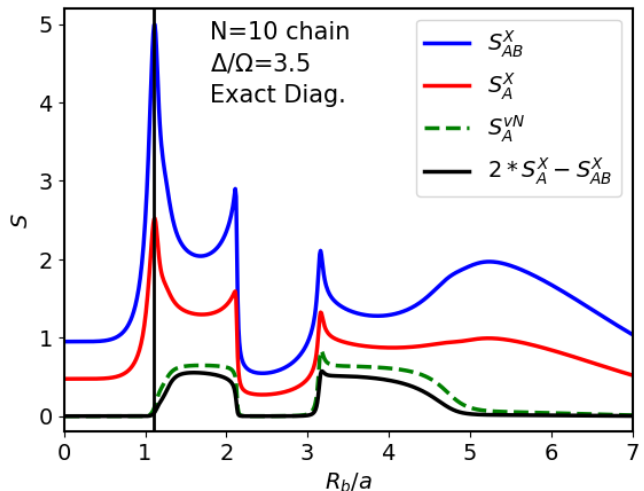


FIG. 1. Entropies for a chain of 10 atoms with $\Delta/\Omega = 3.5$ as a function of R_b/a_x : S_{AB}^X , $S_A^X = S_B^X$, $I_{AB}^X = 2S_A^X - S_{AB}^X$, and S_A^{vN} ; the vertical line is at $R_b/a_x = 1.11$;

We observe that S_{AB}^X has approximately the same shape as S_A^X with a constant of proportionality which is approximately 2. In addition $S_A^{vN} \simeq 1.25(2S_A^X - S_{AB}^X)$. As shown in the SM, the proportionality factor is only approximate, for instance, S_A^{vN} is slightly below (above) this linear combination for smaller (larger) R_b/a_x respectively. Notice that as R_b/a_x is increased from low values, the onset of S_A^{vN} is marked by a sharp increase S_{AB}^X and S_A^X . However, at the peak of S_{AB}^X and S_A^X ,

for $R_b/a_x \simeq 1.11$, cancellations occur and S_A^{vN} develops only after S_{AB}^X and S_A^X drop significantly. As expected, $S_A^X \geq S_A^{vN}$ but typically $S_A^X \gg S_A^{vN}$ so this upper bound is not very useful. Other features of Fig. 6 can be understood from elementary considerations that are provided in the SM [38]. In summary, we found that whenever S_A^{vN} is not too small, $I_{AB}^X \simeq 0.8 \times S_A^{vN}$ which is 20 percent below the target value. When S_A^{vN} is small, I_{AB}^X provide a bound that is not so close. Consequently, the mutual information provides a good estimation of the regions of the phase diagram where S_A^{vN} gets large.

Analog simulations. We have repeated parts of the above numerical calculations using the empirical probabilities provided by the Aquila device and the associated Amazon Braket local simulator. As explained in Appendix A, this imposes size constraints not present in exact diagonalization. Calculations for $1.0 \lesssim R_b/a_x \lesssim 2$ can be performed with the local simulator and, for a slightly shorter range of R_b/a_x , with Aquila. In both cases, we ramped up the vacuum adiabatically starting with all atoms in the atomic ground state, increasing Ω and then Δ , exactly as in [37] and illustrated in Appendix A. The data is publicly available [39]. The results are shown in Fig. 2 where we see good estimates of $2S_A^X - S_{AB}^X$ with Aquila. The local simulator becomes less accurate when $R_b/a_x \simeq 2$ and the ramping down of Ω at the end involves subtleties discussed in the SM [38]. Fig. 2 only shows results with no ramping down of Ω at the end for the local simulator.

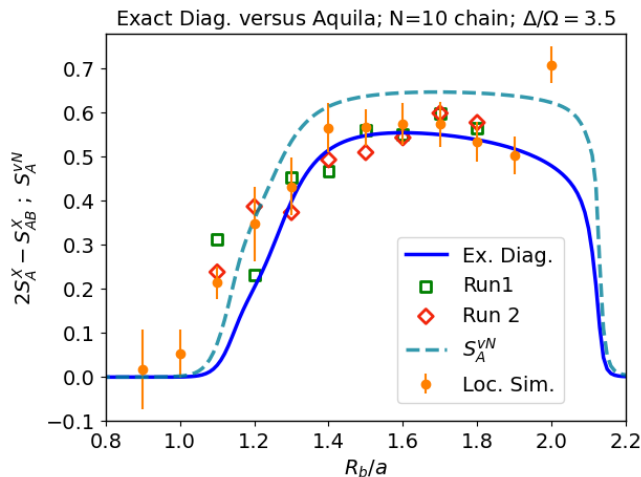


FIG. 2. $2S_A^X - S_{AB}^X$ vs. R_b/a_x with three methods: 1) exact diagonalization (continuous curve); 2) local simulator with no ramping down of Ω at the end (filled circles), the errors bars are calculated using 10 independent runs of 1000 shots; 3) 2 runs with 1000 shots with Aquila (empty symbols); S_A^{vN} (dashed line) is also given for reference.

In Appendix B, we explain that the Aquila values for both S_{AB}^X and $2S_A^X$ are significantly larger than the accurate numerical values, however these errors appear to cancel in I_{AB}^X . In the SM [38], we show that “filtering” the low probabilities tend to increase I_{AB}^X and get it closer

to S_A^{vN} . This is discussed in more detail in Ref. [29].

How tight is the lower bound? So far our model calculation shows that the mutual information I_{AB}^X follows rather closely and from below the von Neuman entanglement entropy S_A^{vN} . This is not always the case. An example [40] of state $|\psi\rangle$ with $I_{AB}^X = 0$ and $S_A^{vN} = \ln 2$ is

$$|\psi\rangle = \frac{1}{2}(|gg\rangle + |gr\rangle + |rg\rangle - |rr\rangle). \quad (9)$$

This state can be obtained by starting with a product state of two $(|g\rangle + |r\rangle)/\sqrt{2}$ and then applying the entangling unitary transformation $\exp(i\pi n_1 n_2)$. All the $p_{\{n\}}$ for both states are 1/4 and the mutual information is zero, but S_A^{vN} changes from zero to $\ln 2$ when the sign of the coefficient of $|rr\rangle$ changes. A discussion of the exactly solvable two qubit case is given in the SM [38].

In order to get a better idea about the generic tightness of the bound, we have repeated our numerical calculations over a broad range of values of Δ/Ω . The results are shown in Fig. 3. We see that the shapes of the heatmaps of S^{vN} and I_{AB}^X are very similar. The ratio I_{AB}^X/S^{vN} reach maximal values of 0.91 in regions where S_A^{vN} is large and small values in regions where S^{vN} is close to 0. This confirms our previous observations that I_{AB}^X delimitates reliably the regions of the phase diagram where S_A^{vN} takes its largest values. We have repeated some of the numerical calculations discussed above with two-leg ladders with five rungs and varied the lattice spacings in both directions. We found very similar features that are reported in the SM [38].

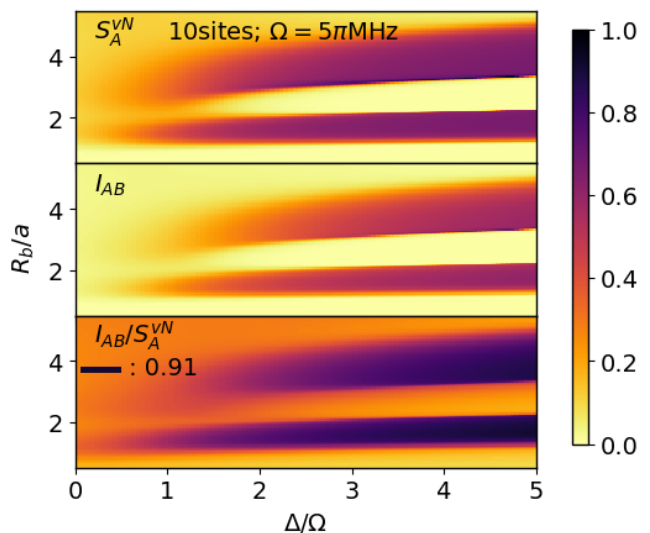


FIG. 3. S_A^{vN} , I_{AB}^X and I_{AB}^X/S_A^{vN} for a 10 sites chain.

Other bitstring proxies. In Ref. [37], we found a detailed correspondence between the contour plots in the $(\Delta/\Omega, R_b/a)$ plane of the peak height of the structure factors, which can be reconstructed from the $p_{\{n\}}$ only, and the contour plots of S_A^{vN} which require the knowledge of the vacuum wave function. This motivated the

idea of finding proxies of S_A^{vN} that depends on the $p_{\{n\}}$ only. Besides I_{AB}^X , one can also construct a second order Rényi version of the S^X quantities defined above:

$$S_{2AB}^X \equiv -\ln \sum_{\{n\}} p_{\{n\}}^2, \text{ and } S_{2A}^X \equiv -\ln \sum_{\{n\}_A} p_{\{n\}_A}^2. \quad (10)$$

As shown in the SM [38], we found numerically that for the 10 atom chain:

$$S_{2A}^R \approx 2S_{2A}^X - S_{2AB}^X. \quad (11)$$

with $S_{2A}^R = -\ln(\text{Tr}\rho_A^2)$. Another possibility is the configurational entanglement entropy. The connection between correlations and purity [41] or the reconstruction of quantum states using a restricted Boltzmann machine based on single-basis measurements [42] could help develop a more general understanding of our observations. Ref. [41] introduces another proxy C for S_A^{vN} in the case of the Bose-Hubbard model called the configurational entanglement entropy. Adapting their definition for the case where the particle number is not conserved and where there is no number entropy, and introducing a function of C that reproduces S_A^{vN} for a two-qubit Bell state we propose to use

$$LC \equiv \ln(1 + \sum_{\{n\}} |p_{\{n\}} - p_{\{n\}_A} p_{\{n\}_B}|). \quad (12)$$

This quantity provides good estimates of S_A^{vN} but has a more intricate behavior which will be discussed separately.

Applications. Arrays of Rydberg atoms have been proposed for quantum simulation of lattice gauge theories [43–52]. More specifically, ladder arrays have been considered as quantum simulators for scalar electrodynamics [47] and their phase diagram has been studied experimentally [37] and with effective Hamiltonian methods [53]. These results show a very rich phase diagram and the need to study the regions of parameter spaces where the correlation lengths are much larger than the lattice spacing (continuum limits). This has possible relevance for the study of inhomogeneous phases and the Lifshitz regime of lattice quantum chromodynamics [54, 55]. Entanglement entropy considerations play an important role in the tentative designs of hybrid algorithms for collider event generators [50].

Generalizations. It is possible to extend our procedure for arbitrary AB partitions where A and B have different sizes. This allows us to study the conjectured lower bound for multipartite entropies which are of great interest in the context of conformal field theory [56–58]. Ongoing calculations show that our proxy provide reasonably tight lower bounds for digitized ϕ^4 models with qudits [30], Ising models in curved space [59] and larger Rydberg arrays than the ones considered here [60].

Conclusions. We have shown that the bitstring mutual information provides robust and reliable estimates for the order of magnitude of the von Neumann entanglement entropy. This works efficiently for a broad range

of adjustable parameters available in arrays of Rydberg atoms. The method can be applied to any qubit based universal or analog quantum computing device. This provides a quick way to map the phase diagram and identify regions of interest from the point of view of approaching continuum limits with quantum simulators.

Appendix A: Analog computation methods

Analog calculations with arrays of Rydberg atoms have been performed with Aquila using the Amazon Braket services. We used the Amazon Braket SDK for local simulations. The actual device imposes constraints not present in exact diagonalization. Analog calculations were performed with a single chain model with 10 sites, $\Omega = 5\pi$ MHz, which implies $R_b = 8.375\mu$, and a detuning $\Delta = 17.5\pi$ MHz. The linear size of the system needs to be less than $100 \mu\text{m}$. This means that we need $R_b/a_x \gtrsim 0.9$. The distance between the atoms needs to be more than $4 \mu\text{m}$ which implies $R_b/a_x \lesssim 2.0$. We used the values $R_b/a_x = 0.9, 1.0, \dots, 2.0$. The ground state needs to be prepared adiabatically and actual measurements with Aquila are performed after turning off Ω . The procedure suggested on the Amazon Braket tutorials lasts $4 \mu\text{s}$ and involves ramping down Ω during the last $0.5 \mu\text{s}$, as illustrated in Fig. 4. This protocol was used for our Aquila calculations. Different ramping down were studied with the local simulator and reported in the SM [38]. We used 1000 shots 10 times for the local simulator and had 2 runs with 1000 shots for Aquila. The raw data files are available in [39].

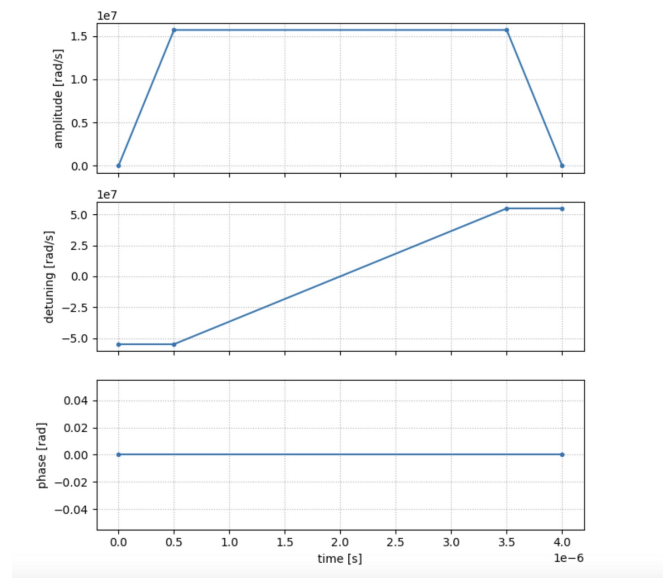


FIG. 4. Standard ramping up or down of Ω (top), Δ (middle) and ϕ (bottom) as appearing in the Amazon Braket notebook tutorials.

Appendix B: Error cancellations

An important aspect of the results presented in Fig. 2 is that the errors (the difference between the analog estimates and the values calculated accurately with numerical methods) for S_{AB}^X and $2S_A^X$ are significant and actually larger than I_{AB}^X . This is illustrated in a specific way in Fig. 5. Near $R_b/a = 1.5$, the difference between Aquila and exact diagonalization for both $2S_A^X$ and S_{AB}^X are both positive and close to 1 while their difference $I_{AB}^X = 2S_A^X - S_{AB}^X$ is of order 0.5 with an estimated error of order 0.1. More details can be found in the SM [38].

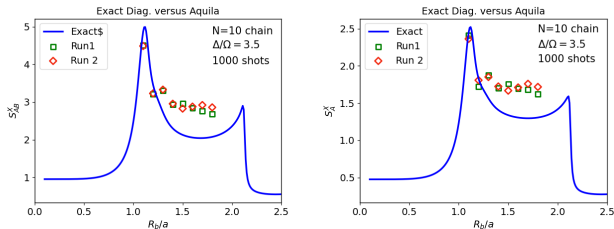


FIG. 5. Top: S_{AB}^X (left), S_A^X (right) vs. R_b/a_x with exact diagonalization (continuous curves) and with Aquila with 2 runs of 1000 shots.

ACKNOWLEDGEMENTS

This research was supported in part by the Dept. of Energy under Award Number DE-SC0019139. Special thanks to Alex Lukin who pointed out the counterexample of Eq. (9) as well as the importance of understanding the proportionality factor. We thank S. Cantu, M. Asaduzzaman, J. Corona, Cheng Chin, Sheng-Tao Wang, A. Bylinskii, Fangli Liu, J. Zeiher, R. Pisarski, P. Komar, B. Senseman, Z. Ozzello, Avi Kaufman and P. Preiss for comments and support. We thank J. Preskill and M. Soleimanifar for pointing out the connection between our empirical bound and the Holevo bound. We thank the Amazon Web Services and S. Hassinger for facilitating remote access to QuEra through the Amazon Braket while teaching quantum mechanics and our Department of Physics and Astronomy for supporting the cost of the analog simulations presented here. The final version was completed while attending the workshop “Co-design for Fundamental Physics in the Fault-Tolerant Era” at the InQubator for Quantum Simulation, University of Washington, Seattle, USA.

SUPPLEMENTARY MATERIAL

In this supplementary material we provide more information about:

- 1: Symmetric bi-partite Hilbert spaces
- 2: Detailed features of the entropies for chains with $\Delta/\Omega = 3.5$
- 3: Entropy errors
- 4: Entropies for a 5 rung ladder and $\Delta/\Omega = 3.5$
- 5: Verification of the bound for two qubits
- 6: Other bitstring proxies

1. Symmetric bi-partite Hilbert space

In the following we consider N_q two-state systems (qubits), for instance an array of Rydberg atoms either in the ground $|g\rangle$ or Rydberg $|r\rangle$ state. For simplicity, we assume that N_q is even and that the whole system (AB) can be divided in two subsystems A and B that can be mapped into each other by some reflection symmetry. A simple example is a linear chain of equally spaced Rydberg atoms with an even number of atoms.

The computational basis consists of the 2^{N_q} elements

$$|\{n\}\rangle \equiv |n_0, n_1, \dots, n_{N_q-1}\rangle, \quad (\text{B1})$$

with $n_j = 0$ or 1. Any element of this basis can be factored in a bi-partite way with the two subsystems of identical size A and B (each with $N_q/2$ qubits)

$$|\{n\}_{AB}\rangle = |\{n\}_A\rangle |\{n\}_B\rangle, \quad (\text{B2})$$

with

$$|\{n\}_A\rangle \equiv |n_0, n_1, \dots, n_{N_q/2-1}\rangle \quad \text{and} \quad (\text{B3})$$

$$|\{n\}_B\rangle \equiv |n_{N_q/2}, \dots, n_{N_q-1}\rangle \quad (\text{B4})$$

Given an arbitrary prepared state $|\psi\rangle$, we can expand it in the computational basis

$$|\psi\rangle = \sum_{\{n\}} c_{\{n\}} |\{n\}\rangle, \quad (\text{B5})$$

and the state $|\{n\}\rangle$ will be observed with a probability

$$p_{\{n\}} = |c_{\{n\}}|^2. \quad (\text{B6})$$

These probabilities can be estimated by measurements and define an ‘‘experimental’’ entropy

$$S_{AB}^X \equiv - \sum_{\{n\}} p_{\{n\}} \ln(p_{\{n\}}), \quad (\text{B7})$$

associated with the state $|\psi\rangle$. It is clear that this quantity depends on the computational basis and that it contains no information about entanglement.

We now define a reduced probability in the subsystem A by tracing over B :

$$p_{\{n\}_A} = \sum_{\{n\}_B} p_{\{n\}_A\{n\}_B}, \quad (\text{B8})$$

and the corresponding reduced entropy

$$S_A^X \equiv - \sum_{\{n\}_A} p_{\{n\}_A} \ln(p_{\{n\}_A}). \quad (\text{B9})$$

Again, this quantity depend on the computational basis used and cannot be identified with the von Neuman entropy S_A^{vN} .

In the following we focus on the case where $|\psi\rangle = |vac.\rangle$, the vacuum of the Hamiltonian. Starting with

$$\rho_{AB} = |vac.\rangle \langle vac.|\quad (\text{B10})$$

and writing the 2^{N_q} dimensional vector $c_{\{n\}}$ corresponding to the vacuum as a $2^{N_q/2} \times 2^{N_q/2}$ matrix

$$C_{\{n\}_A, \{n\}_B} = c_{\{n\}}, \quad (\text{B11})$$

we find that the reduced density matrix $\rho_A = Tr_B \rho_{AB}$ can be written as

$$\rho_{A\{n\}_A, \{n'\}_A} = (CC^\dagger)_{\{n\}_A, \{n'\}_A}, \quad (\text{B12})$$

in the computational basis. The von Neuman entropy is

$$S_A^{vN} = - \sum_m \lambda_m \ln(\lambda_m), \quad (\text{B13})$$

with λ_m the eigenvalues of ρ_A which are independent of the basis used in A .

2. Detailed features of the entropies for chains with $\Delta/\Omega = 3.5$

Several features of Fig. 6 (here, Fig. 1 in the main text) can be understood from elementary considerations. For $R_b/a_x = 0.5$, we have essentially 10 decoupled atoms. Each of the single-atom ground states have a probability $\cos(\theta/2)^2 = 0.981$ (with $\theta = \arctan(\Omega/\Delta)$) to be in the $|r\rangle$ state and the entropy per atom is 0.0951. Numerically we found $S_{AB}^X = 0.9616 \simeq 2S_A^X$ with 3 significant digits while S_A^{vN} is negligible. Near $R_b/a_x=1$, S_{AB}^X and S_A^X increase rapidly to reach maxima near $R_b/a_x = 1.1$ with $S_{AB}^X = 4.874 \simeq 2S_A^X = 4.901$. The most probable state is $|rrrrrrrrrr\rangle$ with a probability of 0.036. For $R_b/a_x = 1.5$, there are four states with probabilities larger than 0.1: $|rggrgrgrgr\rangle$, $|rgrgrgrgrgr\rangle$ (0.138) and $|rgrgrgrgrgr\rangle$ $|rgrgrgrgrgr\rangle$ (0.276). After tracing over the right part, there are three significant probabilities for $|rggrg\rangle$, $|rgrgg\rangle$, and $|rgrgr\rangle$ and $2S_A^X - S_{AB}^X = 0.549$ while $S_A^{vN} = 0.638$. For $R_b/a_x = 2.5$, the state $|rggrgrgrgr\rangle$ has a probability 0.888 and both $2S_A^X - S_{AB}^X$ and S_A^{vN} are small.

Fig. 7 shows that this inequality is verified for chains of size $N_s = 2, 4, \dots 10$. For $N_s = 10$, the fraction of S_A^{vN} not accounted by $2S_A^X - S_{AB}^X$ is compatible with the proportionality factor 1.25 used previously.

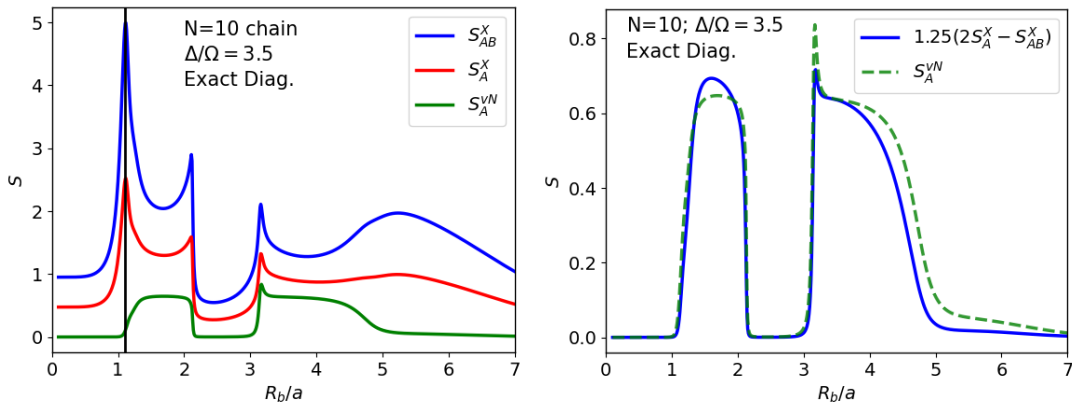


FIG. 6. Entropies for a chain of 10 atoms with $\Delta/\Omega = 3.5$ as a function of R_b/a_x . Top: S_{AB}^X , S_A^X and S_A^{vN} ; the vertical line is at $R_b/a_x = 1.11$; Bottom: $1.25(2S_A^X - S_{AB}^X)$ and S_A^{vN} .

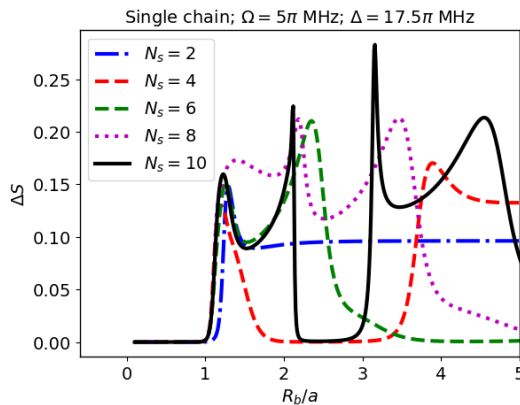


FIG. 7. $S_A^{vN} - (2S_A^X - S_{AB}^X)$ as a function of R_b/a_x for chains of size $N_s = 2, 4, \dots, 10$.

3. Entropy errors

In this supplemental information section, we compare the errors for the local simulator with no ramping down (LSNRD), the local simulator with the standard ramping down (LSST) as in Fig. 4 in the main text, and the actual device Aquila.

We started with the local simulator and found some dependence on the details of the ramping down of Ω at the end. The local simulator allows us to try time sequences not possible with the actual device. In order to check that the adiabatic preparation is working well, we first considered the situation with $\Omega(t)$ flat at the end (so 5π MHz after 4μ sec instead of ramping down to zero after 3.5μ sec as in Fig. 4 in the main text). We used 1000 shots and repeated the experiment ten times in order to estimate the statistical errors. The results are shown in Fig. 8 and show good agreement with exact diagonalization. Except for $R_b/a_x = 1.1, 1.2$ and 2.0 , the values $1.25(2S_A^X - S_{AB}^X)$ obtained with the local simulator agree with less than one standard deviation with the exact diagonalization results. This gives us confidence in the adiabatic preparation of the ground state.

We repeated the local simulation with the realistic ramping down at the end shown in Fig. 4 in the main text. The results are shown in Fig. 9. The agreement is not as good as in Fig. 8. The size of the statistical errors bars are much smaller than the discrepancies with exact diagonalization for S_{AB}^X and S_A^X . However the error somehow cancel in $2S_A^X - S_{AB}^X$ and we obtain reasonable estimates of S_A^{vN} .

We repeated parts of these simulations with the actual device and we can now compare the estimations of S_{AB}^X and S_A^X obtained with: 1) exact diagonalization, 2) the local simulator with no ramping down (LSNRD) as in Fig. 8, 3) the local simulator with the standard ramping down (LSST) as in Fig. 9, and 4) the actual device Aquila. We focus the discussion on $R_b/a_x = 1.5$. In cases 2), 3) and 4) we used two independent runs with 1000 shots. By dividing the number of events by 1000, we obtain estimations of the probabilities that can be calculated exactly.

The results involving more than 10 counts are shown in Table I and lead to the conclusions that:

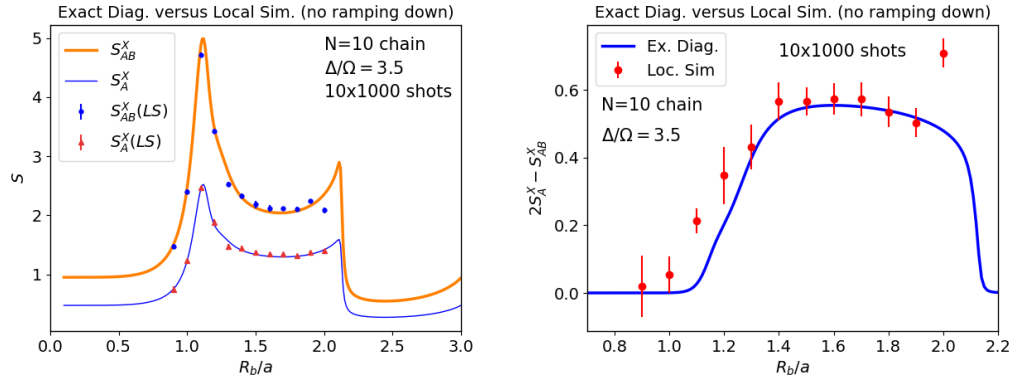


FIG. 8. Left: S_{AB}^X and S_A^X vs. R_b/a_x with exact diagonalization (continuous curves) and the local simulator with no ramping down of Ω at the end (symbols) using 1000 shots 10 times. The errors bars are present but barely visible on the graph. Right: $1.25(2S_A^X - S_{AB}^X)$ with the same conventions. As the vertical scale is five times smaller, the errors bars are clearly visible.

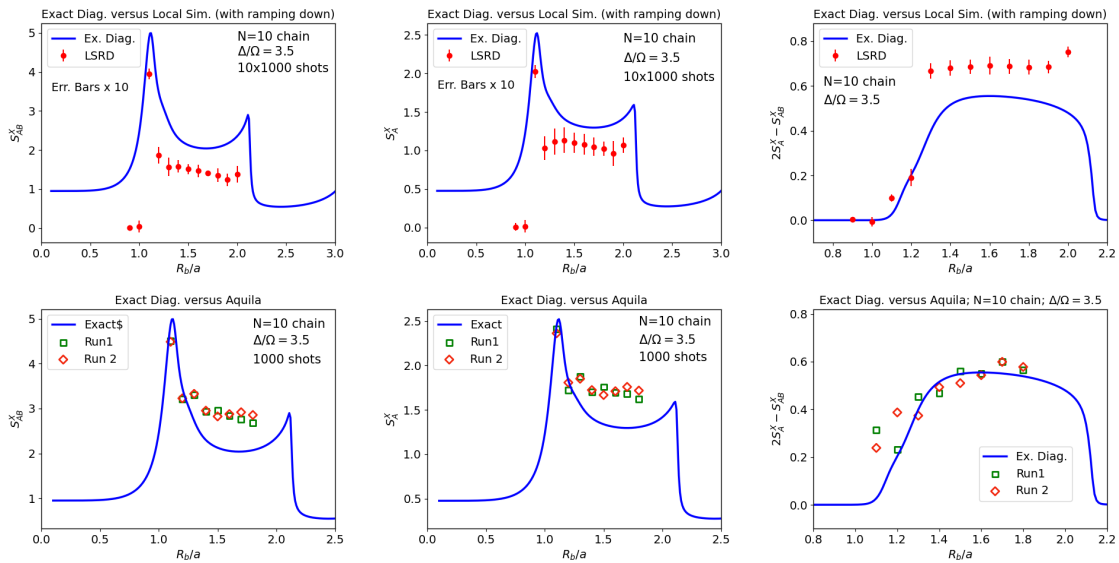


FIG. 9. Top: S_{AB}^X (left), S_A^X (middle) and $2S_A^X - S_{AB}^X$ (right) vs. R_b/a_x with exact diagonalization (continuous curves) and the local simulator with ramping down of Ω at the end as in Fig. 4 in the main text (symbols) using 1000 shots 10 times. The errors bars are multiplied by 10. Bottom: same quantities with Aquila with 2 runs of 1000 shots.

- LSQRD provides reasonably accurate estimations of the probabilities for states in the computational basis, for a broad range of values for the probabilities. This is not a surprise, it just shows that the local simulator works properly.
- LSST removes states with low probabilities and significantly amplifies some medium probabilities such as 0.138 for rgrgrgrgr and rgrgrgrgr. This suggests that a more rapid ramping down maybe preferable for entropy estimation.
- Aquila amplifies some of the low probability states and depletes higher probability states while keeping some ratios roughly in line with exact results.

From the above discussion, it is clear that there are significant fluctuations for states that are expected to be seen 10 times or less in 1000 shots. LSST removes these states while Aquila amplifies them. This suggests to discard results with low counts and proceed with truncated data sets. In the following we considered truncated data sets where states with 10 or less measurements were discarded. By doing this, the number of shots is reduced which leads to different probability estimates. The results of this truncation for the entropies are shown in Table II. From these results we conclude that

- The truncation lowers the entropies calculated with exact diagonalization by about 20 percent but increases $1.25(2S_A^X - S_{AB}^X)$ by about 10 percent.
- LSNRD follows closely the exact results. Again this was expected.
- LSST is insensitive to the truncation. The LSST values are close to exact truncated values. Again this was expected.
- Aquila results are very sensitive to truncation which brings the results closer to exact ones, but maybe not as close as hoped.

More generally, the truncation method seems to introduce significant uncertainties and we believe that error cancellations with the untruncated procedure may be more reliable.

Method State	Exact	LSNRD1	LSNRD2	LSST1	LSST2	Aquila1	Aquila2
grgrgrgrgr	12	14	19	24	18	16	18
rggggrgrgr	16	21	18	< 10 (0)	< 10 (1)	15	14
rggrgrgrgr	138	142	152	201	222	136	149
rgrgggrgrgr	23	18	28	< 10 (0)	< 10 (0)	19	24
rgrgrgrgg	< 10 (6)	11	< 10 (7)	< 10 (0)	< 10 (0)	14	< 10 (5)
rgrgrgrgr	276	232	239	274	264	174	175
rgrgrgggr	16	14	18	< 10 (0)	< 10 (0)	19	12
rgrgrgrgr	276	248	244	278	266	190	180
rgrgrgrgr	138	179	168	207	200	151	179
rgrgrgrgrg	12	13	18	12	25	23	16
Total	907	892	904	996	995	804(*)	812(**)

TABLE I. States with at least 10 observations for 1000 shots. For Aquila, (*) five additional states are not in the table: ggrgrgrgr (12), rgggrgrgr (12), rggrgrgggr (12), rgrgggrgr (14), rgrgrgrgr (11) for run 1, and (**) and three additional states are not in the table: rgggrgrgr (12), rggrgggrgr (11), rgrgrgrgg (12) for run 2.

Method Entropy	Exact	LSNRD1	LSNRD2	LSST1	LSST2	Aquila1	Aquila2
S_{AB}^X	2.126	2.241	2.198	1.527	1.558	2.944	2.874
$S_{AB}^X(\text{Trunc.})$	1.6476	1.734	1.740	1.504	1.527	2.035	1.901
S_A^X	1.337	1.374	1.354	1.117	1.134	1.685	1.681
$S_A^X(\text{Trunc.})$	1.131	1.149	1.167	1.115	1.108	1.288	1.233
$1.25(2S_A^X - S_{AB}^X)$	0.686	0.634	0.639	0.883	0.888	0.531	0.611
$1.25(2S_A^X - S_{AB}^X)(\text{Trunc.})$	0.769	0.706	0.742	0.907	0.861	0.676	0.707

TABLE II. Entropies calculated with the full data set and truncated data sets (Trunc.) where observations with less than 10 events are discarded.

4. Entropies for a 5 rung ladder and $\Delta/\Omega = 3.5$

We repeated the calculation for ladder-shaped arrays with 5 rungs and 2 legs and different aspect ratios. We found very similar results for the same approximate constant 1.25 as shown in Fig. 10. Fig. 11 makes clear that the inequality

$$S_A^{vN} \geq 2S_A^X - S_{AB}^X, \quad (\text{B14})$$

holds.

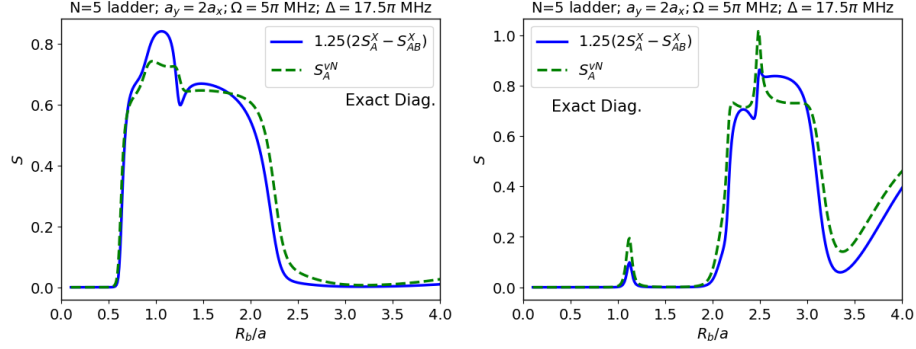


FIG. 10. $1.25(2S_A^X - S_{AB}^X)$ and S_A^{vN} as a function of R_b/a_x for $a_y = 0.5a_x$ (left) and $a_y = 2a_x$ (right).

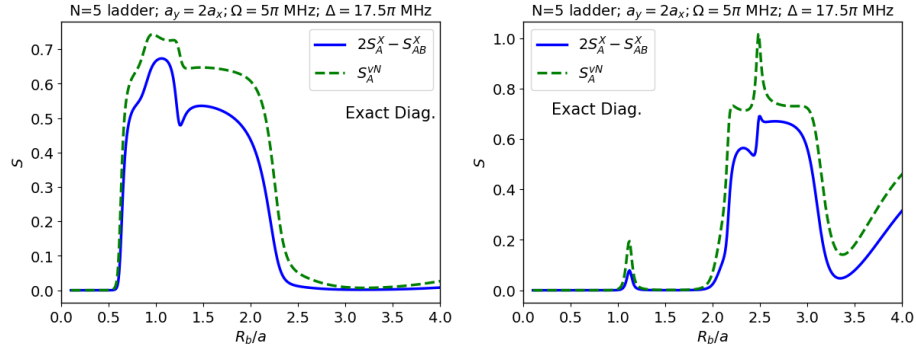


FIG. 11. $2S_A^X - S_{AB}^X$ and S_A^{vN} as a function of R_b/a_x for $a_y = 0.5a_x$ (left) and $a_y = 2a_x$ (right).

5. Verification of the bound for two qubits

In this section, we consider a general two-qubit state

$$|\psi\rangle = \sum_{n_1 n_2=0,1} c_{n_1 n_2} |n_1 n_2\rangle. \quad (\text{B15})$$

The reduced two by two density matrix can be calculated exactly and we obtain

$$S_A^{vN} = - \sum_{\pm} \lambda_{\pm} \ln(\lambda_{\pm}), \quad (\text{B16})$$

with

$$\lambda_{\pm} = \frac{1}{2}(1 \pm \sqrt{1 - 4\text{Det}}), \quad (\text{B17})$$

with the determinant

$$\text{Det} = p_{01}p_{10} + p_{00}p_{11} - 2\sqrt{p_{00}p_{11}p_{01}p_{10}} \cos(\xi), \quad (\text{B18})$$

and a complex phase

$$\exp(i\xi) = (c_{00}c_{11}c_{01}^*c_{10}^*)/|c_{00}c_{11}c_{01}c_{10}|. \quad (\text{B19})$$

Det increases when ξ increases from 0 to π . $S_A^{vN} = 0$ when Det=0 and $\ln 2$ when Det=1/4 and in general increases with Det. Consequently, we have the inequality

$$S_A^{vN}(p_{\{n\}}, \xi) \geq S_A^{vN}(p_{\{n\}}, \xi = 0). \quad (\text{B20})$$

The inequality

$$S^{vN}(|c_{n_1 n_2}\rangle, \xi = 0) \geq 2S_A^X - S_{AB}^X. \quad (\text{B21})$$

is verified numerically in Fig. 12 using spherical coordinates to parametrize the norms of the coefficients expressed in spherical coordinates $|c_{00}| = \cos \phi \sin \theta$; $|c_{11}| = \sin \phi \sin \theta$; $|c_{01}| = |c_{10}| = \cos \theta / \sqrt{2}$ with $0 \leq \theta, \phi \leq \pi/2$. This enforces the constraint that the probabilities add to one.

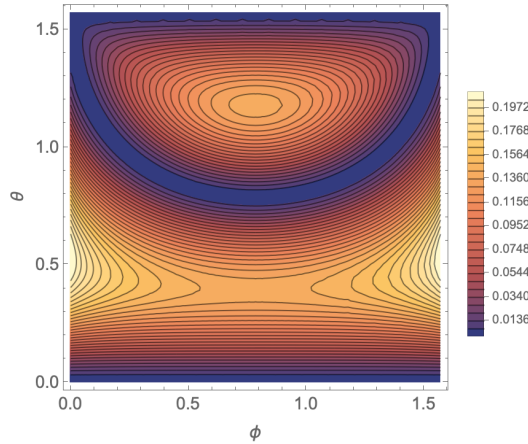


FIG. 12. $S^{vN}(\xi = 0) - (2S_A^X - S_{AB}^X)$ for two qubits using the spherical coordinates described in the text.

6. Other bitstring proxies

The adapted bitstring entropies for the second order Rényi entropies can be defined as

$$S_{2AB}^X \equiv -\ln \sum_{\{n\}} p_{\{n\}}^2, \text{ and } S_{2A}^X \equiv -\ln \sum_{\{n\}_A} p_{\{n\}_A}^2. \quad (\text{B22})$$

We can then compare $2S_{2A}^X - S_{2AB}^X$ with the quantum second order Rényi entropy $S_{2A}^R = -\ln(\text{Tr}\rho_A^2)$. The numerical results for a 10 atom chain using exact diagonalization are displayed in Fig. 13. This provides support for

$$2S_{2A}^X - S_{2AB}^X \approx S_{2A}^R. \quad (\text{B23})$$

However, it appears that $2S_{2A}^X - S_{2AB}^X$ is not always positive.

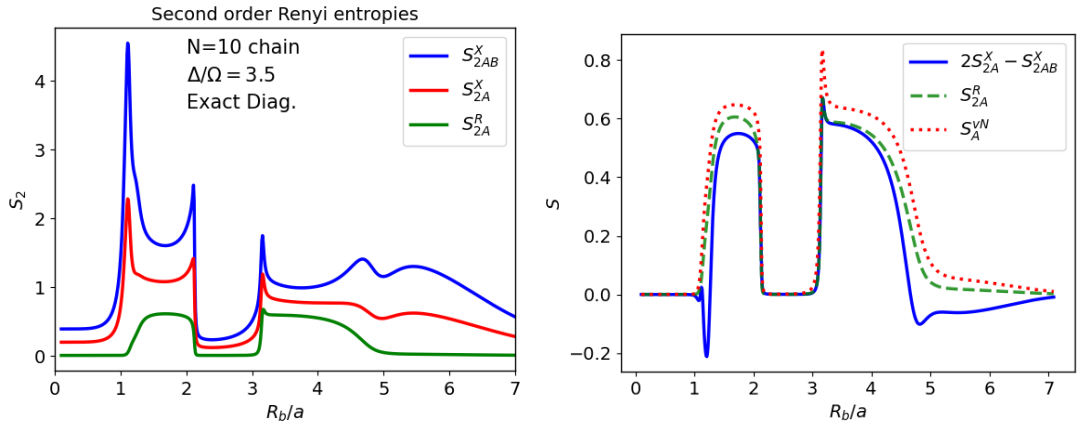


FIG. 13. Second order Rényi entropies. Left: S_{2AB}^X (top), S_{2A}^X (middle) and S_{2A}^R (bottom) ; Right: $2S_{2A}^X - S_{2AB}^X$, S_{2A}^R , and S_A^{vN} for a chain of 10 atoms with $\Delta/\Omega = 3.5$ as a function of R_b/a_x .

We also considered the adapted configurational entropy

$$C \equiv \sum_{\{n\}} |p_{\{n\}} - p_{\{n\}_A} p_{\{n\}_B}|, \quad (\text{B24})$$

and the modified version introduced in the main text:

$$LC \equiv \ln\left(1 + \sum_{\{n\}} |p_{\{n\}} - p_{\{n\}_A} p_{\{n\}_B}|\right). \quad (\text{B25})$$

This quantity provides good estimates of S_A^{vN} but is not always a lower bound.

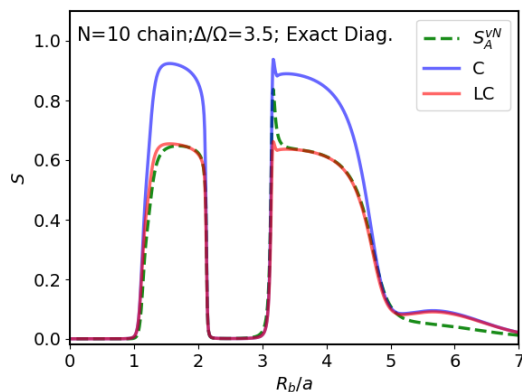


FIG. 14. C , LC , and S_A^{vN} for a chain of 10 atoms with $\Delta/\Omega = 3.5$ as a function of R_b/a_x .

-
- [1] L. Amico, R. Fazio, A. Osterloh, and V. Vedral, Entanglement in many-body systems, *Reviews of Modern Physics* **80**, 517 (2008).
- [2] J. Eisert, M. Cramer, and M. B. Plenio, Area laws for the entanglement entropy - a review, *Rev. Mod. Phys.* **82**, 277 (2010), arXiv:0808.3773 [quant-ph].
- [3] D. A. Abanin, E. Altman, I. Bloch, and M. Serbyn, Colloquium : Many-body localization, thermalization, and entanglement, *Reviews of Modern Physics* **91**, 10.1103/revmodphys.91.021001 (2019).
- [4] J. I. Cirac, D. Perez-Garcia, N. Schuch, and F. Verstraete, Matrix product states and projected entangled pair states: Concepts, symmetries, theorems, *Rev. Mod. Phys.* **93**, 045003 (2021), arXiv:2011.12127 [quant-ph].
- [5] S. Ghosh, R. M. Soni, and S. P. Trivedi, On The Entanglement Entropy For Gauge Theories, *JHEP* **09**, 069, arXiv:1501.02593 [hep-th].
- [6] K. Van Acoleyen, N. Bultinck, J. Haegeman, M. Marien, V. B. Scholz, and F. Verstraete, The entanglement of distillation for gauge theories, *Phys. Rev. Lett.* **117**, 131602 (2016), arXiv:1511.04369 [quant-ph].
- [7] M. C. Bañuls, K. Cichy, J. I. Cirac, K. Jansen, and S. Kühn, Efficient basis formulation for 1+1 dimensional $SU(2)$ lattice gauge theory: Spectral calculations with matrix product states, *Phys. Rev. X* **7**, 041046 (2017), arXiv:1707.06434 [hep-lat].
- [8] J. Knaute, M. Feuerstein, and E. Zohar, Entanglement and confinement in lattice gauge theory tensor networks, *JHEP* **02**, 174, arXiv:2401.01930 [quant-ph].
- [9] D. E. Kharzeev and E. M. Levin, Deep inelastic scattering as a probe of entanglement, *Phys. Rev. D* **95**, 114008 (2017), arXiv:1702.03489 [hep-ph].
- [10] O. K. Baker and D. E. Kharzeev, Thermal radiation and entanglement in proton-proton collisions at energies available at the cern large hadron collider, *Phys. Rev. D* **98**, 054007 (2018).
- [11] K. Zhang, K. Hao, D. Kharzeev, and V. Korepin, Entanglement entropy production in deep inelastic scattering, *Phys. Rev. D* **105**, 014002 (2022), arXiv:2110.04881 [quant-ph].
- [12] S. R. Beane, D. B. Kaplan, N. Klco, and M. J. Savage, Entanglement Suppression and Emergent Symmetries of Strong Interactions, *Phys. Rev. Lett.* **122**, 102001 (2019), arXiv:1812.03138 [nucl-th].
- [13] C. Robin, M. J. Savage, and N. Pillet, Entanglement Rearrangement in Self-Consistent Nuclear Structure Calculations, *Phys. Rev. C* **103**, 034325 (2021), arXiv:2007.09157 [nucl-th].
- [14] G. Vidal, J. I. Latorre, E. Rico, and A. Kitaev, Entanglement in quantum critical phenomena, *Phys. Rev. Lett.* **90**, 227902 (2003).
- [15] V. E. Korepin, Universality of entropy scaling in one dimensional gapless models, *Phys. Rev. Lett.* **92**, 096402 (2004).
- [16] P. Calabrese and J. L. Cardy, Entanglement entropy and quantum field theory: A Non-technical introduction, *Int. J. Quant. Inf.* **4**, 429 (2006), arXiv:quant-ph/0505193.
- [17] S. Ryu and T. Takayanagi, Holographic derivation of entanglement entropy from AdS/CFT, *Phys. Rev. Lett.* **96**, 181602 (2006), arXiv:hep-th/0603001.
- [18] D. A. Abanin and E. Demler, Measuring entanglement entropy of a generic many-body system with a quantum switch, *Phys. Rev. Lett.* **109**, 020504 (2012).
- [19] A. J. Daley, H. Pichler, J. Schachenmayer, and P. Zoller, Measuring entanglement growth in quench dynamics of bosons in an optical lattice, *Phys. Rev. Lett.* **109**, 020505 (2012).
- [20] R. Islam, R. Ma, P. M. Preiss, M. Eric Tai, A. Lukin, M. Rispoli, and M. Greiner, Measuring entanglement entropy in a quantum many-body system, *Nature* **528**, 77–83 (2015).
- [21] A. M. Kaufman, M. E. Tai, A. Lukin, M. Rispoli, R. Schittko, P. M. Preiss, and M. Greiner, Quantum thermalization through entanglement in an isolated many-body system, *Science* **353**, 794–800 (2016).
- [22] J. Unmuth-Yockey, J. Zhang, P. M. Preiss, L.-P. Yang, S. W. Tsai, and Y. Meurice, Probing the conformal Calabrese-Cardy scaling with cold atoms, *Phys. Rev. A* **96**, 023603 (2017), arXiv:1611.05016 [cond-mat.quant-gas].
- [23] C. Shannon and W. Weaver, *The Mathematical Theory of Communication* (University of Illinois Press, 1998).
- [24] M. A. Nielsen and I. L. Chuang, *Quantum Computation and Quantum Information: 10th Anniversary Edition*

- (Cambridge University Press, 2011).
- [25] J. Preskill, Quantum information chapter 10. quantum shannon theory (2022).
- [26] J. Wurtz, A. Bylinskii, B. Braverman, J. Amato-Grill, S. H. Cantu, F. Huber, A. Lukin, F. Liu, P. Weinberg, J. Long, S.-T. Wang, N. Gemelke, and A. Keesling, Aquila: Quera’s 256-qubit neutral-atom quantum computer (2023), arXiv:2306.11727 [quant-ph].
- [27] E. Witten, A Mini-Introduction To Information Theory, Riv. Nuovo Cim. **43**, 187 (2020), arXiv:1805.11965 [hep-th].
- [28] J. Preskill and M. Soleimanifar, Private communication (2024).
- [29] A. Kaufman, J. Corona, Z. Ozzello, M. Asaduzzaman, and Y. Meurice, Improved entanglement entropy estimates from filtered bitstring probabilities (2024), arXiv:2411.07092 [quant-ph].
- [30] Z. Ozzello and Y. Meurice, Work in progress (2024).
- [31] H. Bernien, S. Schwartz, A. Keesling, H. Levine, A. Omran, H. Pichler, S. Choi, A. S. Zibrov, M. Endres, M. Greiner, V. Vuletić, and M. D. Lukin, Probing many-body dynamics on a 51-atom quantum simulator, Nature **551**, 579 (2017).
- [32] A. Keesling, A. Omran, H. Levine, H. Bernien, H. Pichler, S. Choi, R. Samajdar, S. Schwartz, P. Silvi, S. Sachdev, P. Zoller, M. Endres, M. Greiner, V. Vuletić, and M. D. Lukin, Quantum kibble–zurek mechanism and critical dynamics on a programmable rydberg simulator, Nature **568**, 207 (2019).
- [33] H. Labuhn, D. Barredo, S. Ravets, S. de Léséleuc, T. Macrì, T. Lahaye, and A. Browaeys, Tunable two-dimensional arrays of single rydberg atoms for realizing quantum ising models, Nature **534**, 667 (2016).
- [34] S. de Léséleuc, V. Lienhard, P. Scholl, D. Barredo, S. Weber, N. Lang, H. P. Büchler, T. Lahaye, and A. Browaeys, Observation of a symmetry-protected topological phase of interacting bosons with rydberg atoms, Science **365**, 775 (2019).
- [35] S. Ebadi, T. T. Wang, H. Levine, A. Keesling, G. Semeghini, A. Omran, D. Bluvstein, R. Samajdar, H. Pichler, W. W. Ho, S. Choi, S. Sachdev, M. Greiner, V. Vuletić, and M. D. Lukin, Quantum phases of matter on a 256-atom programmable quantum simulator, Nature **595**, 227 (2021).
- [36] P. Scholl, M. Schuler, H. J. Williams, A. A. Eberharter, D. Barredo, K.-N. Schymik, V. Lienhard, L.-P. Henry, T. C. Lang, T. Lahaye, A. M. Läuchli, and A. Browaeys, Quantum simulation of 2d antiferromagnets with hundreds of rydberg atoms, Nature **595**, 233 (2021).
- [37] J. Zhang *et al.*, Probing quantum floating phases in Rydberg atom arrays, Nature Commun. **16**, 712 (2025), arXiv:2401.08087 [quant-ph].
- [38] Y. Meurice, Supplementary material (2024).
- [39] Zenodo repository, <https://zenodo.org/records/15103785> (2025).
- [40] This was pointed out to us by Alex Lukin.
- [41] A. Lukin, M. Rispoli, R. Schittko, M. E. Tai, A. M. Kaufman, S. Choi, V. Khemani, J. Léonard, and M. Greiner, Probing entanglement in a many-body–localized system, Science **364**, 256–260 (2019).
- [42] G. Torlai, B. Timar, E. P. van Nieuwenburg, H. Levine, A. Omran, A. Keesling, H. Bernien, M. Greiner, V. Vuletić, M. D. Lukin, R. G. Melko, and M. Endres, Integrating neural networks with a quantum simulator for state reconstruction, Physical Review Letters **123**, 10.1103/physrevlett.123.230504 (2019).
- [43] J. Zhang, J. Unmuth-Yockey, J. Zeiher, A. Bazavov, S.-W. Tsai, and Y. Meurice, Quantum simulation of the universal features of the polyakov loop, Phys. Rev. Lett. **121**, 223201 (2018).
- [44] F. M. Surace, P. P. Mazza, G. Giudici, A. Lerose, A. Gambassi, and M. Dalmonte, Lattice gauge theories and string dynamics in rydberg atom quantum simulators, Phys. Rev. X **10**, 021041 (2020).
- [45] S. Notarnicola, M. Collura, and S. Montangero, Real-time-dynamics quantum simulation of (1+1)-dimensional lattice qed with rydberg atoms, Phys. Rev. Res. **2**, 013288 (2020).
- [46] A. Celi, B. Vermersch, O. Viyuela, H. Pichler, M. D. Lukin, and P. Zoller, Emerging Two-Dimensional Gauge Theories in Rydberg Configurable Arrays, Phys. Rev. X **10**, 021057 (2020), arXiv:1907.03311 [quant-ph].
- [47] Y. Meurice, Theoretical methods to design and test quantum simulators for the compact Abelian Higgs model, Phys. Rev. D **104**, 094513 (2021), arXiv:2107.11366 [quant-ph].
- [48] P. Fromholz, M. Tsitsishvili, M. Votto, M. Dalmonte, A. Nersesyan, and T. Chanda, Phase diagram of rydberg-dressed atoms on two-leg triangular ladders, Phys. Rev. B **106**, 155411 (2022).
- [49] D. González-Cuadra, T. V. Zache, J. Carrasco, B. Kraus, and P. Zoller, Hardware Efficient Quantum Simulation of Non-Abelian Gauge Theories with Qudits on Rydberg Platforms, Phys. Rev. Lett. **129**, 160501 (2022), arXiv:2203.15541 [quant-ph].
- [50] K. Heitritter, Y. Meurice, and S. Mrenna, Prolegomena to a hybrid Classical/Rydberg simulator for hadronization (QuPYTH) (2022), arXiv:2212.02476 [quant-ph].
- [51] C. W. Bauer *et al.*, Quantum Simulation for High-Energy Physics, PRX Quantum **4**, 027001 (2023), arXiv:2204.03381 [quant-ph].
- [52] J. C. Halimeh, M. Aidelsburger, F. Grusdt, P. Hauke, and B. Yang, Cold-atom quantum simulators of gauge theories (2023), arXiv:2310.12201 [cond-mat.quant-gas].
- [53] J. Zhang, S. W. Tsai, and Y. Meurice, Critical behavior of lattice gauge theory Rydberg simulators from effective Hamiltonians, Phys. Rev. D **110**, 034513 (2024), arXiv:2312.04436 [quant-ph].
- [54] R. D. Pisarski, V. V. Skokov, and A. M. Tselik, A Pedagogical Introduction to the Lifshitz Regime, Universe **5**, 48 (2019).
- [55] T. Kojo, Y. Hidaka, L. McLerran, and R. D. Pisarski, Quarkyonic chiral spirals, Nuclear Physics A **843**, 37 (2010).
- [56] M. Headrick and T. Takayanagi, A Holographic proof of the strong subadditivity of entanglement entropy, Phys. Rev. D **76**, 106013 (2007), arXiv:0704.3719 [hep-th].
- [57] P. Hayden, M. Headrick, and A. Maloney, Holographic Mutual Information is Monogamous, Phys. Rev. D **87**, 046003 (2013), arXiv:1107.2940 [hep-th].
- [58] T.-C. Lin and J. McGreevy, Conformal Field Theory Ground States as Critical Points of an Entropy Function, Phys. Rev. Lett. **131**, 251602 (2023), arXiv:2303.05444 [hep-th].
- [59] M. Asaduzzaman, S. Catterall, A. Maloney, Y. Meurice, A. Samlodia, and G. C. Toga, Work in progress (2024).
- [60] J. Corona, M. Asaduzzaman, and Y. Meurice, Work in progress (2024).